Characteristics of Turbulent Round Jets in its Potential-Core Region

S. Sivakumar, Ravikiran Sangras and Vasudevan Raghavan

Abstract—In this work, stationary hot-wire measurements are carried out to investigate the characteristics of a round free jet in its potential core region ($0 \leq x/d \leq 10$). Measurements are carried out on an incompressible round jet for a range of Reynolds numbers from 4000 to 8000, calculated based on the jet exit mean velocity and the nozzle diameter. The effect of flow velocity on the development characteristics of the jet in the core region is analyzed. Time-averaged statistics, spectra of velocity and its higher order moments are presented and explained.

Keywords—Contoured nozzle, hot-wire anemometer, Reynolds number, velocity fluctuations, velocity spectra.

I. INTRODUCTION

JETS emerging from round nozzles into un-confined surroundings are useful in several areas of technical interest. Jet flows are encountered in a variety of engineering applications including combustion, chemical processes, pollutant discharge, cooling process, mixing and drying processes. The structure and development of turbulent jets were studied by many researchers [1,2,3]. The near-field development and spectra of turbulent jets were reported by a few authors [4,5], where it was concluded that the near-field region is susceptible to the variations in initial and boundary conditions. This created a wide area for jet research comprising of different initial and boundary conditions in the near-field of a jet. Studies were reported on turbulent jets, considering the variations in parameters such as the Reynolds number [6], nozzle geometry and turbulent intensity at the nozzle exit [7,8,9,10,11]. The effect of different nozzle intrusions in the jet was studied by a few researchers [12,13,14].

The effect of Reynolds number in the near-field of turbulent round jet had been studied by using stationary and flying hot-wire anemometer [6]. Experiments were carried out for a range of Reynolds numbers, however, detailed results for a Reynolds number of 30000 was reported. It had been observed that the length of potential core decreases with increase in Reynolds number. The effect of Reynolds number on the near-field of a plane jet was also studied [15], where it was reported that multiple frequency peaks prevail in the near-field region at low Reynolds number. It had also been mentioned that plane jets at

Sivakumar S is with the Department of Mechanical Engineering, Indian Institute of Technology Madras, Chennai - 600036 INDIA. (e-mail: ssivakumar.r@gmail.com).

Ravikiran Sangras is with the Department of Mechanical Engineering, Indian Institute of Technology Hyderabad, Yeddumailaram - 502205 INDIA (e-mail: sangras@iith.ac.in).

Vasudevan Raghavan is with the Department of Mechanical Engineering, Indian Institute of Technology Madras, Chennai - 600036 INDIA (phone: +91-44-22574712, email: raghavan@iitm.ac.in).

lower Reynolds numbers never attain isotropy, in contrast to high Reynolds number jets, which attain the isotropic state in the far field (x/d = 140).Researchers have reported significant amount of work in the field of turbulent jets at moderate Reynolds numbers, both in the near- and far-field regions. However, only a very few research works are available to explain the characteristics in a potential core region of turbulent jet. In this paper, an experimental study on incompressible round jets at low Reynolds number is reported, where the main focus is on the transition region of jet within the potential core region. The statistical and temporal changes in the quantities of interest, within the potential core region of the round jet, are presented in detail.

II. EXPERIMENTAL SETUP

A. Experimental Setup and Jet Domain

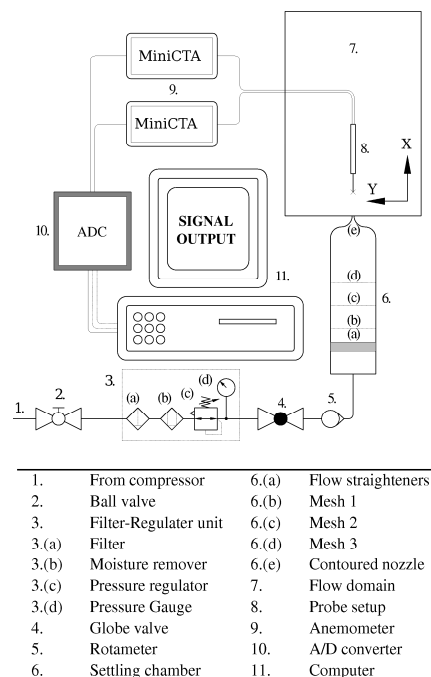A schematic representation of overall experimental setup is shown in Fig. 1.

1.	From compressor	6.(a)	Flow straighteners
2.	Ball valve	6.(b)	Mesh 1
3.	Filter-Regulator unit	6.(c)	Mesh 2
3.(a)	Filter	6.(d)	Mesh 3
3.(b)	Moisture remover	6.(e)	Contoured nozzle
3.(c)	Pressure regulator	7.	Flow domain
3.(d)	Pressure Gauge	8.	Probe setup
4.	Globe valve	9.	Anemometer
5.	Rotameter	10.	A/D converter
6.	Settling chamber	11.	Computer

Fig. 1 Experimental Setup

Compressed air at a constant upstream pressure of 750 kPa, and a flow rate of 0.243 m³/s is supplied from a storage tank of capacity 20 m³ through a pressure regulator and rotameter into a settling chamber. A ball valve is used to open or close the air

circuit securely. The impurities and moisture in the air have been removed by a filter and moisture remover. The settling chamber consists of honeycomb for straightening the flow and meshes having different spacing (mesh 1 - 1 mm, mesh 2 - 0.5 mm, mesh 3 - 0.25 mm), for eliminating the vortices in the flow. The air stream is subjected to axisymmetric contraction using a 5th order contracting nozzle, where the contraction ratio is 400:1. The jet emerging from the nozzle exit is ensured to have low turbulent intensity and an almost top-hat profile. Flow domain is in the shape of a square prism with base dimensions of 0.5 m × 0.5 m and a height of 0.8 m, surrounded by wire mesh of 1 mm spacing. This wire mesh is optimized for having adequate entrainment with minimum disturbances in the entraining air. Hot-wire probe is accurately positioned at any location in the flow domain by using a three-dimensional manual traverse setup having a swept volume of 0.5 m × 0.5 m × 0.5 m.

B. Calibration of Hot-Wire Anemometer

Stationary hot-wire anemometer, having a wire of 10 μm diameter and a length of 1.25 mm, is used to measure transient velocity data at any location within the jet flow field (component 7 in Fig. 1). It is calibrated using the mean velocity data obtained by a stainless steel Pitot tube having a port diameter of 0.5 mm. The mean velocity is calculated from the measured pressure difference, by connecting the Pitot tube to a differential manometer. Errors involved in the x-probe hot-wire calibration, as reported in literature [16], present a relation between the flow velocity, probe angle and the electrical output.

$$E_1{}^2 - E_0{}^2 = AU^n \cos^m(\alpha - \delta) \qquad (1)$$

$$E_2{}^2 - E_0{}^2 = AU^n \cos^m(\alpha + \delta) \qquad (2)$$

In (1) and (2), E_1 and E_2 are the mean voltage measured on the bridge at a given velocity U, from wires 1 and 2, respectively. The voltage obtained at zero velocity is designated as E_0. Further in (1) and (2), α is the angle between the wire and the probe axis, δ is the angle between the mean flow direction and the probe axis, and A, n, and m, are the constants to be determined during calibration.

C. Data Processing

The hot-wire (component 8 in Fig. 1) loses its heat to the ambient air, primarily due to convection and also due to conduction. This will be proportional to the local flow velocity, which will be sensed by the bridge circuit and amplified by servo amplifier in an instantaneous feedback loop (component 9 in Fig. 1). The analog output from MiniCTA is converted to digital form using an analog to digital converter (component 10 in Fig. 1) and fed to a computer (component 11 in Fig. 1). The wire temperature is set to 240ºC by setting a corresponding overheat resistance in MiniCTA. As the Reynolds number considered is low (4000-8000), the sampling

frequency is set at 20 kHz. The number of samples totaling to 100,000 are collected maintaining low-pass filtering frequency at 10 kHz. Data is acquired from the anemometer with the help of National Instruments DAQ card and is controlled by the commercial software, LabVIEW. The obtained electrical data is converted to velocity data using an in-house code developed in FORTRAN. The post processing of the collected data have been done using Qtiplot and MATLAB.

III. Results

A. Statistical Analysis

The development of mean velocity is observed to be almost steady from a top-hat profile at the nozzle exit to bell-shaped profile at an axial distance of 15d from the nozzle exit (Fig. 2).
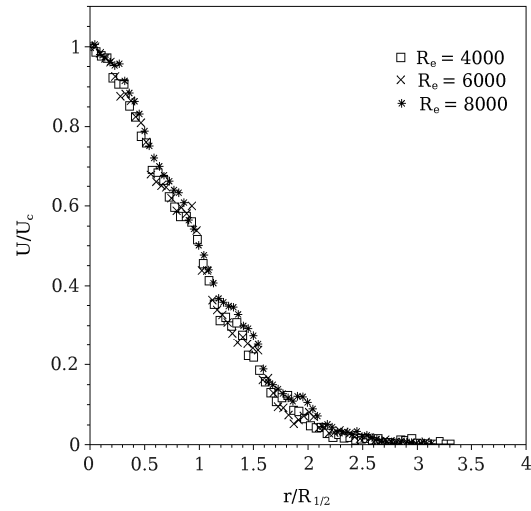

Fig. 2 Mean velocity profile at x/d = 15

There are no significant differences in the velocity profiles between the three different Reynolds number cases. The spread rate of mean velocity is plotted in Fig. 3 in terms of non-dimensional jet half width, $R_{1/2}$ for three Re cases. Clearly, there is zero spread in the potential core region. Mean velocity is measured along the axis of the jet and plotted in Fig. 4. As seen in Fig. 2 in radial profiles, the variations of centre-line velocities are almost the same for the three Re cases, especially in the potential core region, having slight deviations in the near-field region.

A relation to determine the decay constant, as given in equation (3), is reported in literature [6].

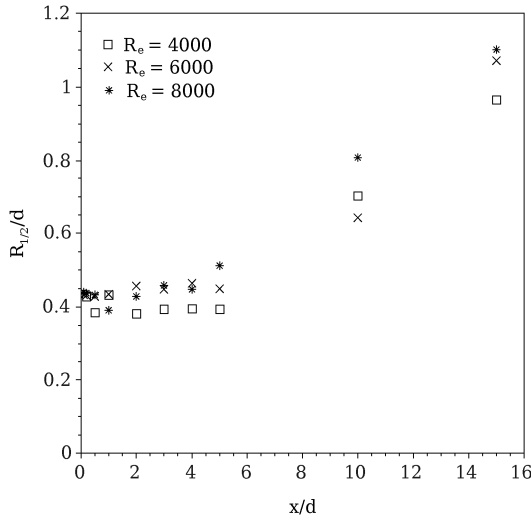$$\frac{U_j}{U_c} = \frac{1}{B}\left(\frac{x}{d} - \frac{x_0}{d}\right) \qquad (3)$$
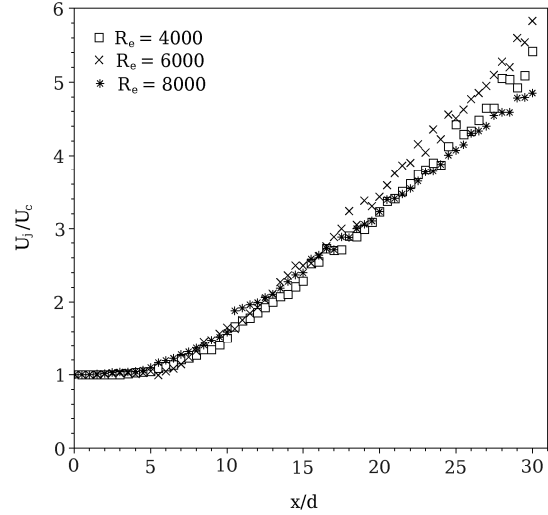
Fig. 3 Spread rate of mean velocity

TABLE I
MEAN VELOCITY DECAY PARAMETERS IN EQUATION (3)

Authors	x/d	x_0/d	B
Present study ($R_e = 6000$)	< 15	2.87	4.83
Fellouah et al. [6]	15 - 29	2.5	5.59
Wygnanski and Fiedler [2]	< 50	3	5.7
	> 50	7	5
Panchapakesan and Lumley [3]	30 - 160	0	6.06
Mi et al. [9]	< 64	3.5	4.48
Xu and Antonia [7]	20 - 75	3.7	5.6
Quinn [8]	18 - 55	2.15	5.9
Abdel Rahman et al. [5]	< 12	1.1±0.39	4.27±4.3

The decay constant and the virtual origin can be estimated from the velocity decay data using (3). These constants have been estimated for the present case with Re=6000, and have been compared with those reported the literature (Table I). The root mean square (rms) value of the velocity data is plotted along the axial direction in Fig. 5. In the near-field region, the rms velocity increases with Re, but in the potential core region, there are no significant differences between the cases. A fully developed turbulent flow has random fluctuations in the flow properties, which closely follow Gaussian distribution [15]. However, in the near-field (transition region) due to non-linear effects, it may not follow the Gaussian distribution.

A dedicated work on PDF analysis with respect to a turbulent jet reported relations for skewness (4) and kurtosis (5) [17].

$$skewness = \left\langle u^3 \right\rangle \big/ \left\langle u^2 \right\rangle^{3/2} \qquad (4)$$

$$kurtosis = \left\langle u^4 \right\rangle \big/ \left\langle u^2 \right\rangle^{2} \qquad (5)$$

Fig. 4 Mean velocity decay

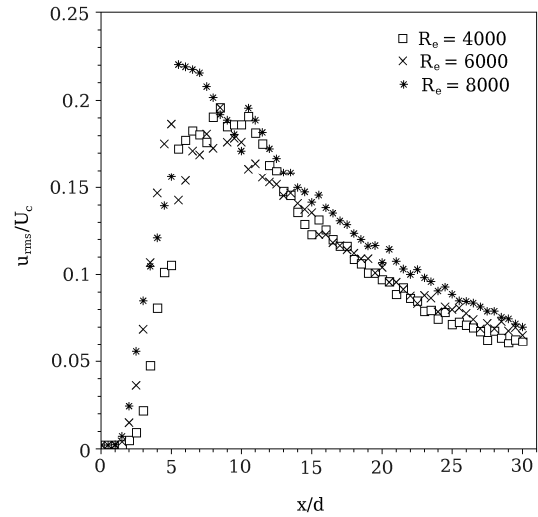

Fig. 5 RMS velocity decay

Radial profiles of these quantities are plotted at six axial locations within the transition region (x/d < 10). The probability density functions are plotted in Fig. 6, for Re values of 4000, 6000 and 8000. It is clearly seen that the radial profiles increasingly deviate from the Gaussian profile as the axial distance is increased within the potential core region. This is due to the instability waves present the potential core region, which dominates without the effect of energy cascading mechanism. The energy cascading mechanism is an energy transfer process in which large eddies break-up into relatively smaller eddies, these smaller eddies undergo a similar break-up process, transferring their energy to yet smaller eddies, continuing till the size of eddy reaches a minimum value at which it is dissipated in to the flow due to viscous effects [18].
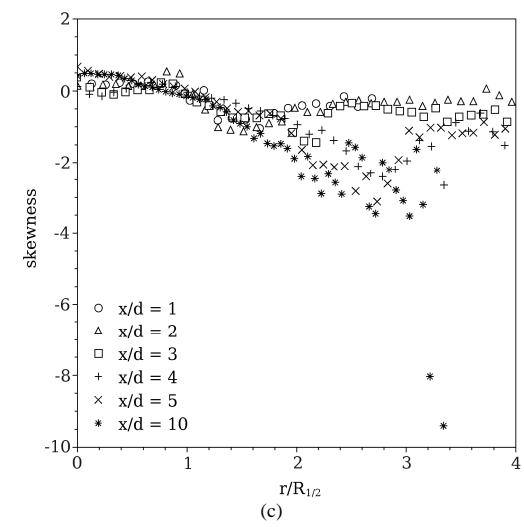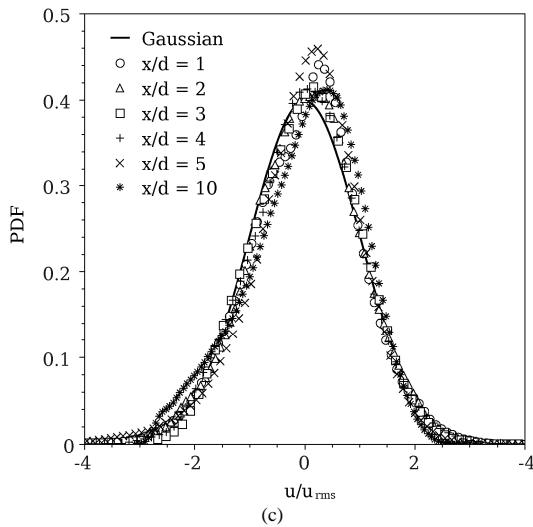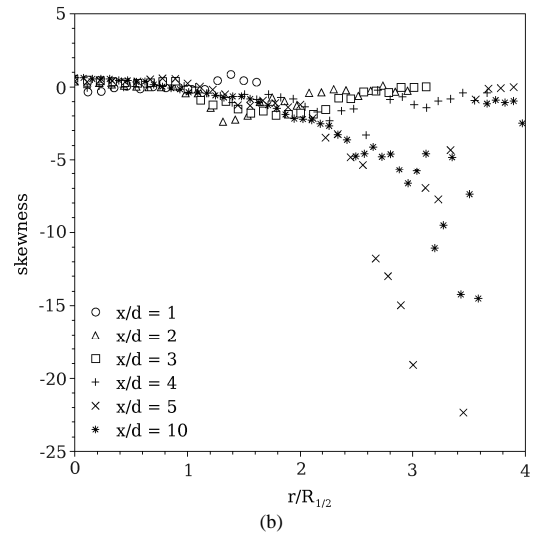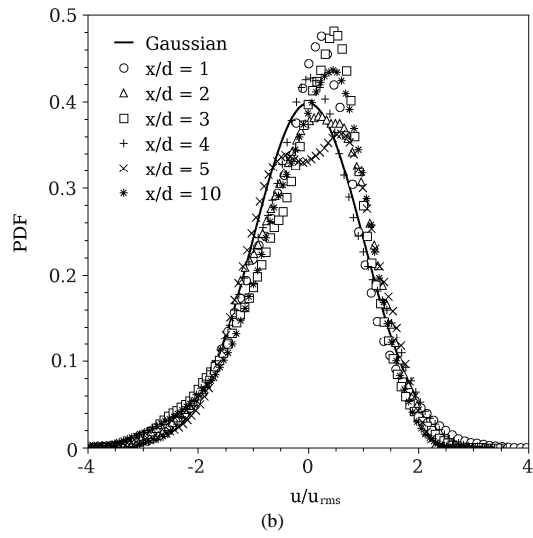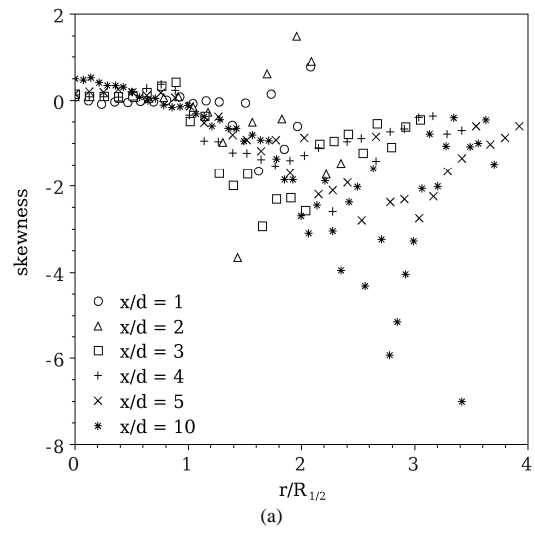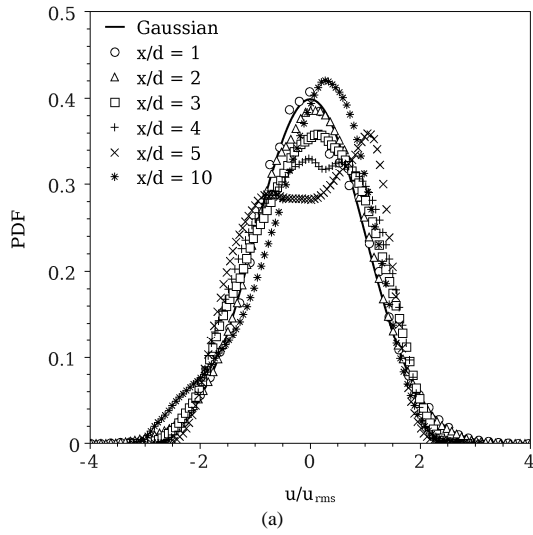
Fig. 6 Probability density functions for three different Reynolds numbers,
(a) 4000, (b) 6000 and (c) 8000

Fig. 7 Skewness for three different Reynolds numbers,
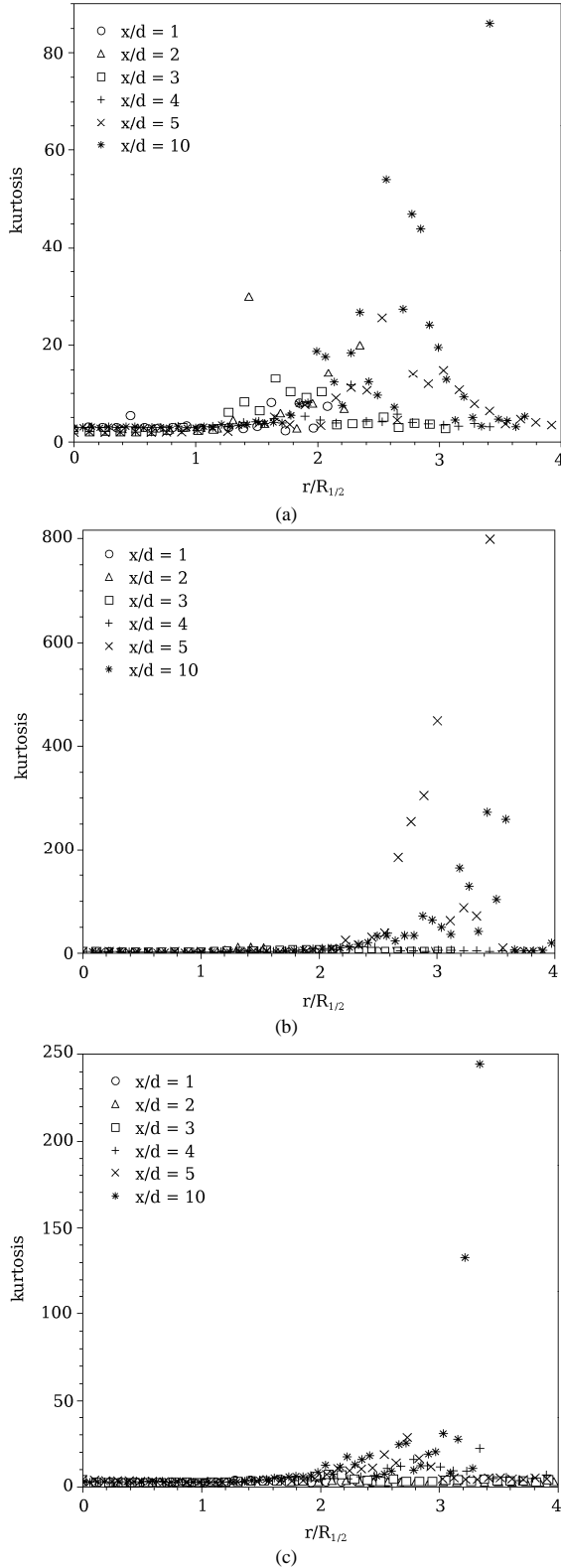(a) 4000, (b) 6000 and (c) 8000

Fig. 8 Kurtosis for three different Reynolds numbers,
(a) 4000, (b), 6000 and (c) 8000

At the axial location of 10d from the nozzle exit, the profile appears to be closer to the Gaussian profile. This is due to the fact that a part of mean flow energy is converted into turbulent kinetic energy, which gets distributed in the form of eddies, thereby enlarging the range of turbulent scales in the flow.

Skewness and kurtosis are plotted along the radial direction in Fig. 7 and Fig. 8, respectively, for three Re cases. Both kurtosis and skewness show peak values at a radial location of around $3R_{1/2}$, denoting a region of intermittency. It is known that at axial locations away from the nozzle exit, the mixing and the randomness increase. However, at an axial location of 5d and at the Re value of 6000, skewness and kurtosis have maximum values.

B. Temporal Analysis

The temporal content of the velocity data is analyzed using fast Fourier transform (FFT). Using 32768 data points, FFT is carried out to determine the entire range of frequencies. It has been plotted for the axial locations in the range of 0.5d to 7.5d, covering the entire potential core region in Fig.9. The effect of Reynolds number is clearly observed in Figs. 9. The frequency scale is made non-dimensional using Strouhal number (fd/U_j). At Re of 4000, Fig. 9(a) shows a single dominating frequency at Strouhal number of 0.26. The amplitude increases till an axial location of around 5.5d, after which multiple peaks are observed. For Re equal to 6000, Fig. 9(b) shows two dominating frequencies, at Strouhal numbers of 1.8 and 3.6. The maximum amplitude occurs for this case at an axial location of 4.5d, after which it decreases gradually and enters into energy cascading. At a still higher Re (8000), Fig. 9(c) shows four dominating frequencies at an axial location of 2d and the energy cascading mechanism starts at 2.5d itself, resulting in the presence of multiple frequencies in this flow region. Similar frequency peaks are observed in literature [15] for plane jet in the near-field region.

One-dimensional energy spectra are investigated at several axial locations within the potential core region (0.5d to 7.5d) and are plotted in Fig. 10. One-dimensional spectra are calculated from the formulae reported in literature [6], as given in (6) and (7).

$$E_{ii}(f) = \int_{-\infty}^{+\infty} e^{-i(2\pi f)\tau} R_{ii}(\tau) d\tau \qquad (6)$$

$$R_{ii} = \int_{-\infty}^{+\infty} u_i(\tau + t)u_i(\tau) d\tau = \overline{u_i(\tau + t)u_i(\tau)} \qquad (7)$$

In this paper, an auto-correlation for velocities, till 0.1 s, is carried out. Fourier transform of the auto-correlation data has been done to get the one-dimensional spectra (axial velocity). Spectra show a similar behavior as that of the FFT analysis. The maxima in spectra at Reynolds numbers of 4000 (Fig. 10(a)) and 8000 (Fig. 10(c)) have completely disappeared at axial location of 7d and 5.5d. For Reynolds number of 6000 (Fig. 10(b)), the maxima are found till an axial location of 7.5d and can possibly extend beyond it.
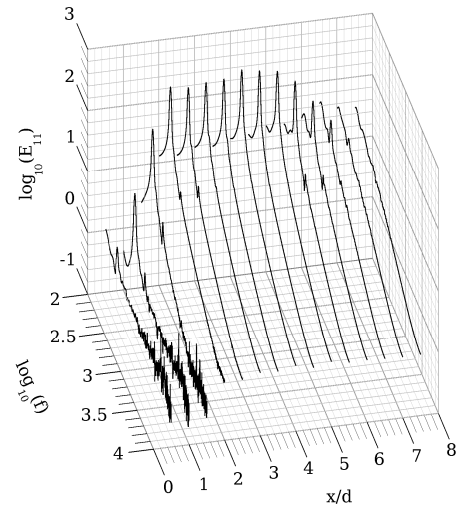
(a)

(a)
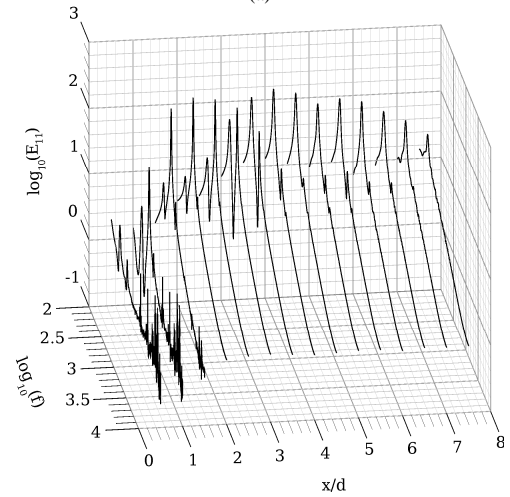

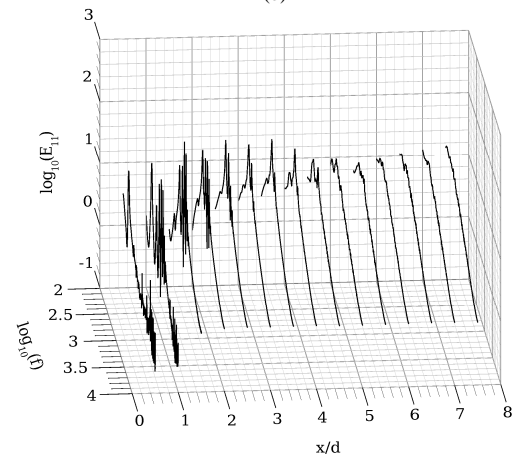(b)
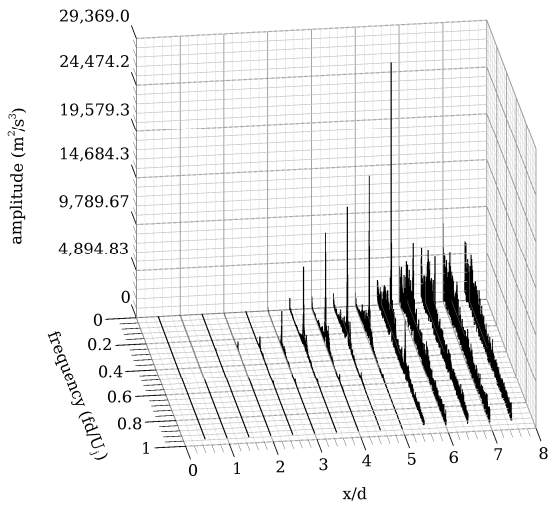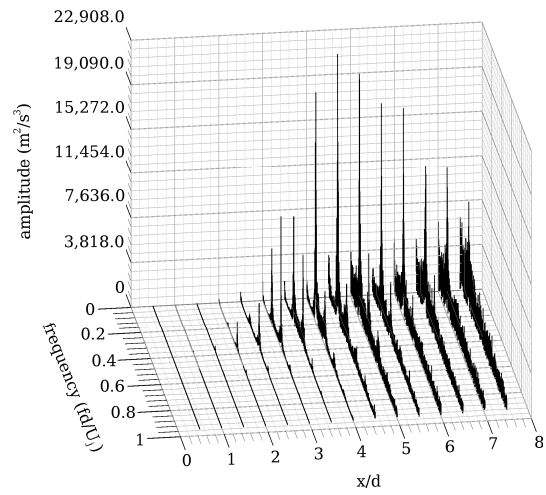
(b)
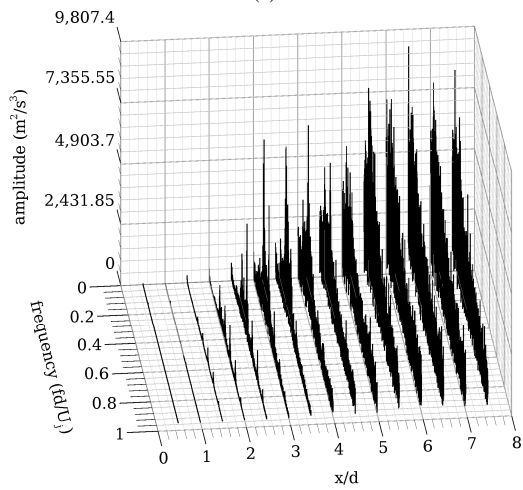
(c)

Fig. 9 Fourier transform of axial velocity for different three
Reynolds numbers, (a) 4000, (b) 6000 and (c) 8000

(c)

Fig. 10 One dimensional spectra at three different Reynolds
numbers,
(a) 4000, (b) 6000 and (c) 8000

IV. CONCLUSION

Potential core region of incompressible round jet has been studied thoroughly by measuring the transient velocity data with the help of hot wire anemometry. The results agree well those available in literature. The mean velocity field in all the three cases shows negligible difference in the near-field region and is almost the same in the potential core region. The nonlinearity behavior in the potential core region is well captured by the PDFs. The intermittency region in the potential core region is clearly shown by the kurtosis and skewness plots, located at a distance of $3R_{1/2}$ radially from the jet axis. An increase in Reynolds number advances the energy cascading mechanism towards nozzle exit. Fourier transform of velocity fluctuations shows the onset of energy cascading mechanism for three different cases. One dimensional spectra of velocity fluctuations shows good variation in the diffusion of kinetic energy for three different Reynolds numbers along the axial direction.

NOMENCLATURE

□	Angle between probe axis and wire, *rad*
A, m, n	Constants in King's law
B	Decay constant
DAQ	Data Acquisition
δ	Angle between probe axis and flow direction, *rad*
d	Nozzle exit diameter, *m*
E_0	Electrical output from wire at zero velocity, *V*
E_1	Electrical output from wire 1 at specific velocity U, *V*
E_2	Electrical output from wire 2 at specific velocity U, *V*
E_{ii}	One dimensional spectra
FFT	Fast Fourier Transform
f	Frequency, *Hz*
h	Grid spacing, *m*
PDF	Probability Density Function
$R_{1/2}$	Half width radius, *m*
R_e	Reynolds number
R_{ii}	Autocorrelation
rms	Root Mean Square
U_c	Mean centerline velocity, *m/s*
U_j	Nozzle exit velocity, *m/s*
u′	Fluctuating axial velocity, *m/s*
v′	Fluctuating radial velocity, *m/s*
u′v′	Reynolds stress, m^2/s^2
x_0	Virtual origin, *m*

REFERENCES

[1] S. Sami, T. Carmody, and H. Rouse, "Jet diffusion in the region of flow establishment," *Journal of Fluid Mechanics*, vol. 27, pp. 231–252, 1967.

[2] I. Wygnanski and H. Fiedler, "Some measurements in the self-preserving jet," *Journal of Fluid Mechanics*, vol. 38, pp. 577–612, 1969.

[3] P. N.R. and J. Lumley, "Turbulence measurements in axisymmetric jets of air and helium. part 1. air jet," *Journal of Fluid Mechanics*, vol. 246, pp. 197–223, 1993.

[4] L. Boguseawski and C. O. Popiel, "Flow structure of the free round turbulent jet in the initial region," *Journal of Fluid Mechanics*, vol. 90, pp. 531–539, 1979.

[5] A.-R. A.A., S. AI-Fahed, and W. Chakroun, "The near-field characteristics of circular of jets at low reynolds numbers," *Mechanics Research Communications*, vol. 23, pp. 313–324, 1996.

[6] F. H., C. Ball, and A. Pollard, "Reynolds number effects within the development region of a turbulent round free jet," *International Journal of Heat and Mass Transfer*, vol. 52, pp. 3943–3954, 2009.

[7] G. Xu and R. Antonia, "Effect of different initial conditions on a turbulent round free jet," *Experiments in Fluids*, vol. 33, pp. 677–683, 2002.

[8] Q. W.R., "Upstream nozzle shaping effects on near field flow in round turbulent free jets," *European Journal of Mechanics B/Fluids*, vol. 25, pp. 279–301, 2006.

[9] J. Mi and G. Nathan, "Statistical properties of turbulent free jets issuing from nine differently-shaped nozzles," *Flow Turbulence Combustion*, vol. 84, pp. 583–606, 2010.

[10] T. Shakouchi, M. Kito, T. Sakamoto, K. Tsujimoto, and T. Ando, "Flow control of jet flow by passive nozzle configuration changes," *International Journal of Flow Control*, vol. 1, pp. 73–85, 2009.

[11] S. Ashforth-Frost and K. Jambunathan, "Effect of nozzle geometry and semi-confinement on the potential core of a turbulent axisymmetric free jet," *Int. Comm. Heat Mass Transfer*, vol. 23, pp. 155–162, 1996.

[12] R. H.R. and T. Wong, "Velocity field characteristics of turbulent jets from round tubes with coil inserts," *Applied Thermal Engineering*, vol. 22, pp. 1037–1045, 2002.

[13] P. Burattini, R. Antonia, S. Rajagopalan, and M. Stephens, "Effect of initial conditions on the near-field development of a round jet," *Experiments in Fluids*, vol. 37, pp. 56–64, 2004.

[14] P. Burattini and L. Djenidi, "Velocity and passive scalar characteristics in a round jet with grids at the nozzle exit," *Flow, Turbulence and Combustion*, vol. 72, pp. 199–218, 2004.

[15] P. Suresh, K. Srinivasan, T. Sundararajan, and S. K. Das, "Reynolds number dependence of plane jet development in the transitional regime," *Physics of Fluids*, vol. 20, p. 044105, 2008.

[16] C. Olinto and S. Möller, "X-probe calibration using collis and william's equation," in *10o Brazilian Congress of Thermal Sciences and Engineering*, 2004.

[17] H. Mouri, M. Takaoka, A. Hori, and Y. Kawashima, "Probability density function of turbulent velocity fluctuations," *Phys. Rev. E*, vol. 65, p. 056304, 2002.

[18] Stephen B. Pope, *Turbulent Flows*, New York: Cambridge University Press, 2000, ch. 6.